

Research Paper**Correspondence to:**

Spyros Pavlides

pavlides@geo.auth.gr**DOI number:**[http://dx.doi.org/10.12681/](http://dx.doi.org/10.12681/bgsg.14334)

bgsg.14334

Keywords:

*Co-seismic ruptures,
earthquake effects,
Coulomb static stress
change*

Citation:

Spyros Pavlides,
Alexandros Chatzipetros,
George Papathanasiou,
George Georgiadis, Sotiris
Sboras and Sotiris
Valkaniotis (2017)
Ground deformation and
fault modeling of the 2016
sequence (24 Aug. – 30
Oct.) in central Apennines
(Central Italy), Bulletin
Geological
Society of Greece, 51,
p.76-112.

Publication History:

Received: 13/08/2017

Accepted: 27/11/2017

Accepted article online:

22/12/2017

The Editor wishes to thank
two anonymous reviewers
for their work with the
scientific reviewing of the
manuscript

©2017. The Author

This is an open access
article under the
terms of the Creative
Commons Attribution
License, which permits
use, distribution and
reproduction in any
medium, provided the
original work is
properly cited

**Ground deformation and fault modeling of the 2016 sequence
(24 Aug. – 30 Oct.) in central Apennines (Central Italy)****Spyros Pavlides** ^(1,2), **Alexandros Chatzipetros** ^(1,2), **George Papathanasiou** ^(1,2), **George Georgiadis** ^(1,2), **Sotiris Sboras** ^(1,3) and **Sotiris Valkaniotis** ^(1,4)

¹ Earthquake Geology Research Team, Geology Department,
A.U.Th. <http://eqgeogr.weebly.com>

² Departments of Geology, Aristotle University of Thessaloniki, Greece

³ Institute of Geodynamics, National Observatory of Athens, Greece

⁴ 42131, Trikala, Greece

pavlides@geo.auth.gr, ac@geo.auth.gr, gpatha@gmail.com, gggk@geo.auth.gr,
ssboras@gmail.com, valkaniotis@yahoo.com

Abstract

A chain fault reactivation took place in central Apennines, from August 24 to October 30, 2016, producing five moderate-to-strong earthquakes ranging from $M_w=5.5$ to $M_w=6.6$. This paper presents the results from the study of the ground co-seismic ruptures around the Monte Vettore and Vettoreto, and Norcia. Surface co-seismic ruptures, were observed in the Vettore and Vettoreto segment of the fault for some kilometres (~7 km) in the August earthquakes, which were partly re-activated and expanded northward during the October earthquakes. Ruptures with 5-15 cm displacements are observed both in scree and weathered mantle (elluvium) and the bedrock, mainly fragmented carbonate rocks with small tectonic surfaces. After the October seismic sequence, the co-seismic displacement doubled and reached more than 50 cm. Oblique low-altitude aerial images were acquired at several sites using a UAV and 3D models were constructed using photogrammetric extrapolation. Numerous observed and mapped rock falls, slides of earth-materials etc., occur mainly along the mountain roads, on artificial slopes. They were studied with preliminary mapping from satellite imagery, and examples are presented of large landslides in the epicentral region with pre- and after- the earthquake images. The first four events are associated with four individual fault segments respectively, all aligned along the mountain-fronts of Mt Gorzano and Mt Vettore. The last fifth and strongest event was the result of linkage and breaching of previously activated fault segments. We modelled the fault segments into five seismic sources in order to calculate the post-sequence static stress changes produced by the five seismic sources

(or source faults) to the surrounding faults (receiver faults). Our results suggest possible triggering effects for neighbouring faults located along the strike of the source faults and delay effects for faults which are directly located either on the footwall or hanging-wall.

Keywords: Co-seismic ruptures, earthquake effects, Coulomb static stress change, dislocation modelling, seismic source, ground deformation, Amatrice, Vettore, Norcia, Italy.

Περίληψη

Μια σειρά ενεργοποίησης ρηγματίων με πέντε μέτριους/ισχυρούς σεισμούς μεγέθους $M_w=5.5$ έως $M_w=6.6$ έλαβε χώρα στα κεντρικά Απέννινα, Ιταλία, μεταξύ της 24ης Αυγούστου έως την 30ης Οκτωβρίου 2016. Η εργασία αυτή παρουσιάζει τα αποτελέσματα από την μελέτη των εδαφικών διαρρήξεων στην περιοχή του Monte Vettore, Vettoreto και Norcia. Επιφανειακές συν-σεισμικές διαρρήξεις παρατηρήθηκαν στα τμήματα Vettore και Vettoreto του ρήγματος για αρκετά χιλιόμετρα (~7 km) μετά τους σεισμούς του Αυγούστου, οι οποίες επανα-δραστηριοποιήθηκαν και επεκτάθηκαν προς βόρεια κατά τους σεισμούς του Οκτωβρίου. Διαρρήξεις με μετατοπίσεις 5-15 cm καταγράφηκαν στα κορημάτα, στον μανδύα αποσάθρωσης και στους σχηματισμούς του υποβάθρου, κυρίως κατακερματισμένα ανθρακικά πετρώματα με μικρές τεκτονικές επιφάνειες. Μετά την σεισμική ακολουθία του Οκτωβρίου, η συν-σεισμική μετατόπιση διπλασιάστηκε και ξεπέρασε τοπικά τα 50 cm. Πλάγιες λήψεις χαμηλού ύψους πάρθηκαν σε διάφορα σημεία με τη χρήση UAV και τρισδιάστατες απεικονίσεις δημιουργήθηκαν με τη χρήση φωτογραμμετρικών μεθόδων. Πολυάριθμες βραχοπτώσεις, κατολισθήσεις και εδαφικές ροές καταγράφηκαν κυρίως σε περιοχές έντονου αναγλύφου και κατά μήκος τεχνητών πρανών του οδικού δικτύου. Η χαρτογράφηση των κατολισθητικών φαινομένων συμπληρώθηκε με τη χρήση δορυφορικών οπτικών εικόνων για την ευρύτερη περιοχή της σεισμικής ακολουθίας. Οι πρώτοι τέσσερις σεισμοί συνδέονται με τέσσερα αντίστοιχα ρηξιγενή τμήματα κατά μήκος των ορεινών όγκων Gorzano και Vettore. Ο τελευταίος και ισχυρότερος σεισμός προήλθε ως αποτέλεσμα της συνένωσης και συνολικής διάρρηξης κάποιων εκ των προηγούμενων τμημάτων. Τα τμήματα των ρηγματίων προσομοιώθηκαν ως πέντε σεισμικές πηγές ώστε να υπολογιστεί η μεταβολή των στατικών τάσεων που προκλήθηκε μετά τη λήξη της σεισμικής ακολουθίας. Τα αποτελέσματα δείχνουν ότι είναι δυνατή η επίσπευση της ενεργοποίησης γειτονικών ρηγματίων που βρίσκονται κατά μήκος και εκατέρωθεν της διεύθυνσης των πέντε σεισμικών πηγών, ενώ ρήγματα που βρίσκονται εγκάρσια στη παράταξη των σεισμικών

πηγών, τόσο στη περιοχή του ανερχόμενου όσο και του κατερχόμενου τεμάχους, πιθανώς να καθυστερήσουν την επαναδραστηριοποίησή τους λόγω πτώσης των τάσεων.

Λέξεις κλειδιά: Συν-σεισμικές διαρρήξεις, εδαφικές παραμορφώσεις, μεταβολή στατικών τάσεων κατά Coulomb, προσομοίωση εδαφικής παραμόρφωσης, σεισμικό ρήγμα, Amatrice, Vettore, Norcia, Ιταλία.

1. Introduction

On August 24, 2016, a seismic activity started in central Apennines to the north of Amatrice town along Vettoreto and Vettore mountains (altitude 2,476 m), concentrated on three active NNW-SSW striking faults (Fig. 1). The sequence included five moderate-to-strong earthquakes spanned in a period of more than two months. The earthquake sequence activated a ca. 60 km-long area around the karstic basins of Norcia and Castelluccio, at an altitude of ~ 1,400 m. The first two events occurred on August 24 with magnitudes Mw 6.2 and Mw 5.6, the next two events occurred on October 26 with magnitudes Mw 5.5 and Mw 6.1, and the fifth and strongest event occurred on October 30 with magnitude Mw 6.6.

The sequence suggests i) the occurrence of a large fault zone consisting of distinctive fault segments involving segment linkage, and ii) earthquake triggering due to stress transfer. The broader area of Central Apennines mountain range is dominated by NE-SW to ENE-WSW extension (e.g. Mariucci & Montone, 2016; Carafa & Bird, 2016), a relatively recent process (e.g. Maliverno & Ryan, 1986; Pucci et al., 2014; Valensise et al., 2016) with a rather slow rate of 2-3 mm/a (Carafa & Bird, 2016). Normal faults regularly bound intramountain karstic basins of pre-orogenic origin (Mesozoic) (e.g. Tavarnelli, 1996; Butler et al., 2006; Scisciani, 2009). As a characteristic faulting style in this region, Valensise et al. (2016) suggest that upward propagation of fault rupture is restricted due to the occurrence of pre-existing regional thrusts or other inherited structural features which act as barriers and/or deflectors. The proposed, by various institutes (INGV, GFZ, GCMT, USGS and IPGP), fault plane solutions (Table 1) of the five strongest events of the 2016 sequence follow the above geodynamic pattern and agree with the NNW-SSE-trending normal fault pattern in the broader area as suggested in previous studies (Calamita & Pizzi, 1992; 1994; Calamita et al., 1992; 1994; Centamore et al., 1992; Blumetti et al., 1993; Boncio & Lavecchia, 2000; Galadini & Galli, 2000; Galadini et al., 2003; Pizzi et al., 2002; Borre et al., 2003; Boncio et al., 2004; Galli et al., 2005; Pace et al., 2006; Pizzi & Galadini, 2009; Pauselli et al., 2010; Pierantoni et al., 2013 and geodatabases like DISS, 2015 and ITHACA, 2000).

The persistent seismic activity of the fault zone with the successive rupturing of its fault segments and the occurrence of other nearby faults, lead us to the calculation of the post-sequence Coulomb static stress changes. To achieve this target, we modelled and evaluated the responsible fault segments of these events.

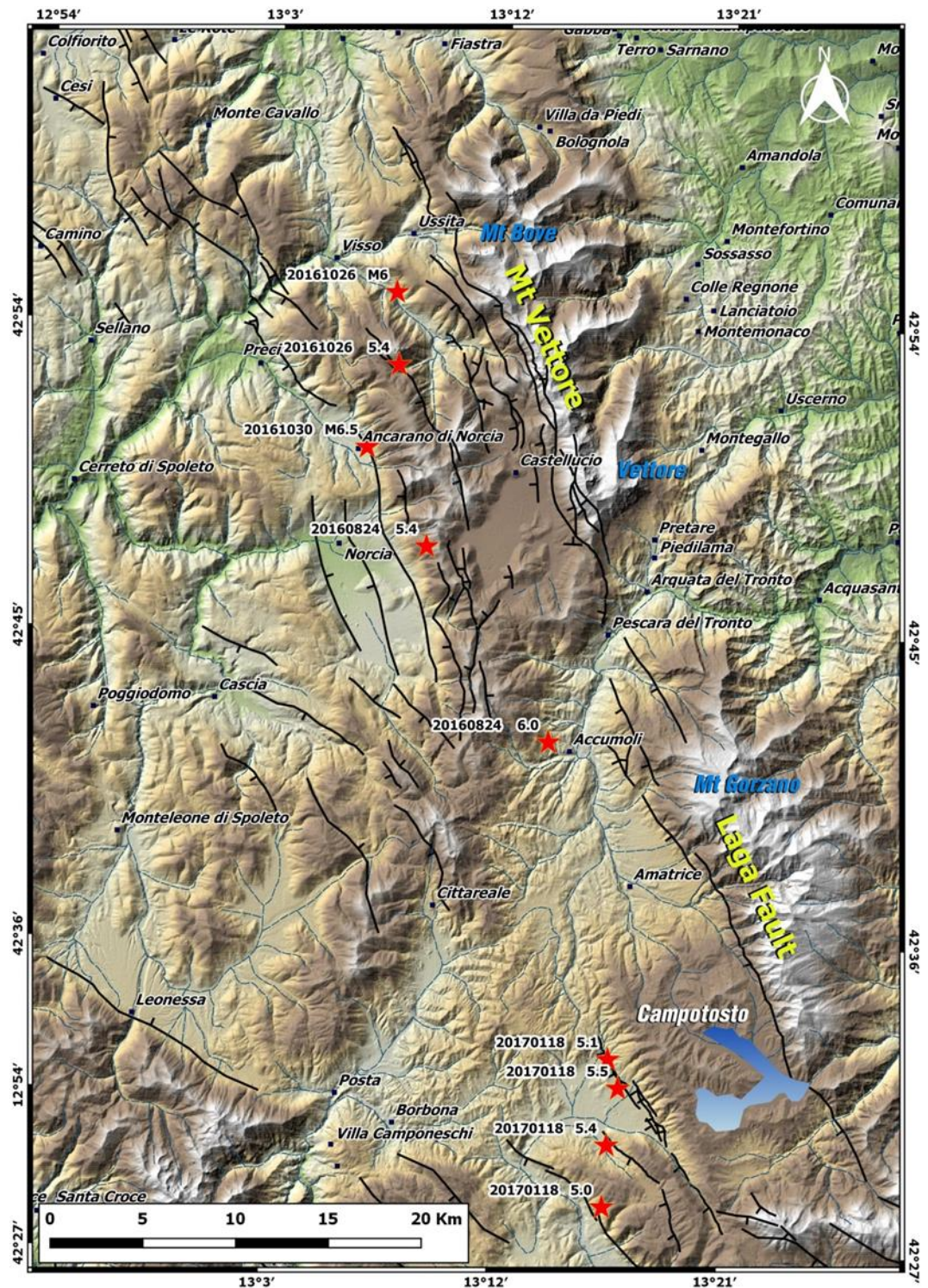


Fig.1. Map of the earthquake region with the seismic NNW-SSW striking faults Mt. Vettore Fault and Laga Fault. Red stars are the $M_w > 5$ epicentres of the earthquake sequence, from CNT-INGV. Main epicentres for the January 18, 2017 aftershock sequence near Campotosto lake are also presented. Towns of Amatrice, Castelluccio village, town of Norcia and the

mountains Garzano, Vettore (altitude 2476 m) are also shown. Quaternary faults (in black lines) from Calamita & Pizzi (1992), ITHACA (2000), Tondi & Cello (2003), Roberts & Michetti (2004), Pierantoni et al. (2013).

Table 1: The proposed focal mechanisms of the five major events of the August-October 2016 seismic sequence.

A/A	Source	Lat N	Long E	Depth (km)	M	M (Nm)	Strike1	dip1	rake1	strike2	dip2	rake2
August 24, 2016, 01:36:32.3 GMT												
1	INGV	42.7063	13.2232	5	6.01	1.07E+18	155	49	-87	331	51	-93
2	GFZ	42.74	13.2	10	6.2	2.20E+18	157	43	-76	320	48	-101
3	CMT	42.66	13.2	12	6.2	2.55E+18	142	45	-106	343	47	-75
4	USGS	42.723	13.188	11.5	6.2	2.45E+18	165	49	-78	328	43	-103
5	IPGP	42.714	13.172	8	6.1	2.00E+18	166	50	-72	319	43	-110
August 24, 2016, 02:33:29.4 GMT												
1	INGV	42.7935	13.1537	5	5.3	1.33E+17	135	47	-98	327	43	-81
2	GFZ	42.84	13.12	10	5.5	2.00E+17	143	44	-82	313	47	-96
3	CMT	42.68	13.15	12	5.6	2.99E+17	127	45	-112	337	49	-70
4	USGS	42.834	13.132	11.5	5.6	2.78E+17	134	56	-96	324	34	-82
October 26, 2016, 17:10:36.2 GMT												
1	INGV	42.8788	13.1287	5	5.4	1.46E+27	161	38	-90	341	52	-90
2	GFZ	42.97	13.13	10	5.5	2.00E+17	173	46	-73	330	46	-105
3	CMT	42.82	13.12	12	5.5	2.47E+17	150	37	-109	353	55	-76
4	USGS	42.857	13.023	10	5.5	2.43E+17	160	38	-89	339	52	-90
5	IPGP	42.866	13.056	6	5.5	1.97E+17	174	39	-59	316	57	-112
October 26, 2016, 19:18:07.2 GMT												
1	INGV	42.9152	13.1278	6	5.9	7.38E+17	159	47	-93	344	43	-87
2	GFZ	43	13.15	10	6.1	1.60E+18	169	46	-66	318	49	-110
3	CMT	42.88	13.11	12	6.1	1.76E+18	142	39	-107	344	53	-76
4	USGS	42.934	13.043	10	6.1	1.84E+18	155	50	-89	333	40	-92
5	IPGP	42.962	13.074	6	6	1.45E+18	178	36	-62	325	59	-108
October 30, 2016, 06:40:18.3 GMT												
1	INGV	42.8398	13.1102	5	6.5	7.07E+18	151	47	-89	330	43	-91
2	GFZ	42.92	13.14	10	6.5	6.80E+18	152	44	-94	338	46	-84
3	CMT	42.76	13.15	12	6.6	1.03E+19	149	38	-102	345	53	-81
4	USGS	42.855	13.088	10	6.6	1.07E+19	162	27	-84	335	63	-93
5	IPGP	42.856	13.089	8	6.5	7.29E+18	165	36	-80	332	54	-98

2. Field observations of co-seismic deformation

The events of August 24, 2016 were associated with a main rupture zone extended along the Vettore and Vettoretto Mts. The rupture zone followed a NNW-SSE striking, W-dipping fault located along the west flank of Mt Vettore's summit (Fig. 2). This fault is known from previous studies and maps. According to seismological and geological data, the sources of both earthquakes correspond to two major fault segments, the Mt. Vettore fault (north) and the northern portion of the Laga fault (south) respectively, which in turn are divided into even smaller fragments (Fig. 1). These two major fault segments demonstrate an overlapping, right-stepping geometry

in the area of Pescara del Tronto and Grisciano valley (Calamita et al., 1992; Pizzi et al., 2017). The Laga (or Amatrice) Fault is a normal fault that bounds the Amatrice and Campotosto plateau and going down at the base of the Mt. Gorzano fault escarpment. This mountain front mainly consists of the Laga Formation (Messinian arenaceous to clay deposits) resting on marls (Marne a Pteropodi Fm.) and marly limestones (Marne con Cerrognia Fm). These formations belong to the Laga Flysch and slope deposits from the degradation of the same material - sandstone and clay.



Fig. 2. The western slope of Mt. Vettore, from a distance, and the normal fault traces, NNW-SSE trending SW-dipping, and in detail the fault scarplet.

The Pescara del Tronto and Grisciano valley (see Fig. 1), is the morphological expression of a strike-slip fault zone (Fig. 3). The role of the inherited strike-slip faulting in the morphotectonics of the region and especially in the seismic activity is still unknown. The western slope of Vettore Fault constitutes of a NNW-SSE trending, W-dipping (Fig. 4 and 5) with a northern termination at Mt. Bove.

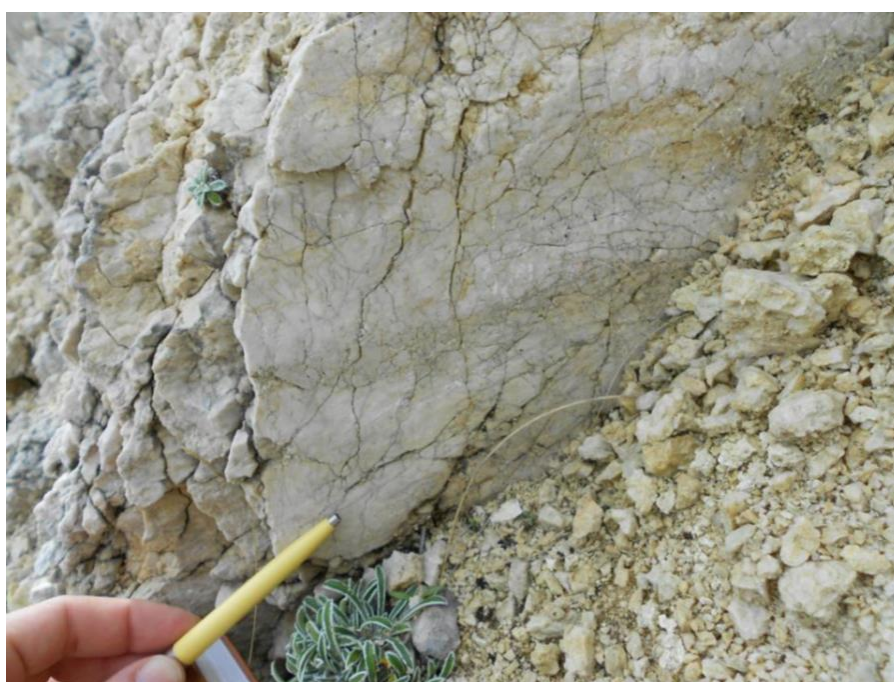


Fig.3. Strike-slip sense of movement on the ENE-trending inherited fault surfaces.



Fig.4. A 3D diagram of Mt Vettore, where the surface ruptures (red line) of the 2016 sequence are shown.

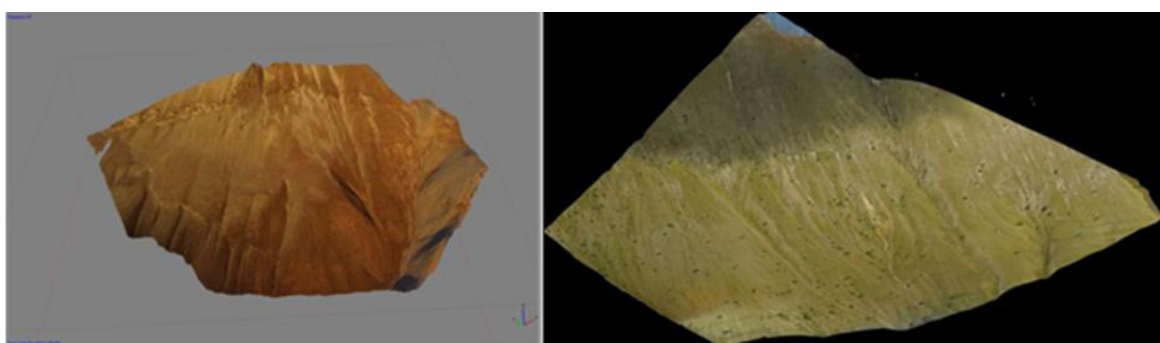


Fig.5. The 3D images derived from the analysis and processing of images shot with UAV (Drone), show in detail the neotectonic faults of the western slope of Mt Vettore, activated during the earthquake sequence.

This slope of the mountain is controlled and deformed by at least two well-constrained major normal faults: the western fault runs along the base of the Vettore escarpment and bounds the Castelluccio basin; and the upper fault crosses close to the top of the Mt. Redentore, marked by a clearly visible fault scarp (known as “Cordone del Vettore”). The deformation from the August event included mainly cracks found in the elluvium adjacent to the fault (Fig. 6). These ground ruptures were up to few cm open and had up to a few cm of normal displacement. They were found in a right stepping, en-echelon geometry with a total length of few meters, striking from NNW-SSE to NW-SE at an angle or sub-parallel to the main fault trace. Single surfaces with vertical displacement not exceeding a few cm were found along the fault trace and also in a 500 m wide zone, perpendicular to the road at the southern slope of Mt

Vettoreto on the hanging-wall of the fault. This was one of the few clear fault-related ruptures, as the ones recorded at the slopes and along the roads of the broader area (Norcia, Amatrice etc.) were generally caused by gravitational sliding and not directly associated with the Vettore fault zone. This is an indication that the actual fault rupture did not reach the surface.

The co-seismic faults of August 24 and that of October 30 were variable in strike, ranging between N140° and N170°, and in dip, ranging between 45° and 70° to the SW. The Mt. Vettore normal fault crosses and displaces the Sibillini thrust fault for some hundreds of metres. This may have locally reutilized some steeper shallow planes of the thrust zone (Pizzi et al., 2017). During our field trips, some distinct ground ruptures along the southern slope of Mt. Vettoreto were surveyed. They are associated with the Mt. Vettore Fault and they strike between NNW and SSE, with a slight left-lateral strike-slip component. The ruptures often follow, or are very close to, the bedrock fault plane (Fig. 7), but sometimes can be found at a distance of several meters. Throw ranges from 1 to 15 cm with heave between 1 and 10 cm (Fig. 6 and 7). The rupture line continues almost uninterruptedly from Mt. Vettoreto slope towards the NW, merging with another fracture line just below the top of Cima Redentore. The ruptures were followed for about 2.5 km, but they extend furthermore to “cordone”, where the total length of this rupture zone is about 4.5 km (Fig. 4).

The October 2016 events reactivated the same fault in Mt Vettore, north of the August manifestations, along with smaller faults in the hanging-wall of this fault. A noticeable coseismic surface was observed along the fault with normal to oblique normal (with left-lateral component) displacement of more than 50 cm (Fig. 8 and 9). The small fault surfaces that were found on the road, at the southern slope of Mt Vettoreto and hanging-wall of the main fault, were reactivated as synthetic and antithetic faults to the main fault with displacements up to several centimetres. Northward, on the slope of Mt Vettore overlooking the Casteluccio plateau, another secondary synthetic fault was activated in the hanging-wall of the main fault. In addition, some minor faults at the western part of the Casteluccio plateau and in the Norcia basin were also activated as synthetic or antithetic to the main Vettore fault, probably as remotely triggered secondary structures, rather than primary ones.

Finally, several probable surface rupture sites were identified by the analysis of interferograms, which, however, could not be verified in the field. The 3D images derived from the analysis and processing of UAV (drone) images, show in detail selected locations with co-seismic rupture; stream, tectonic slope and ruptures of the

08/24/2016 event and the second neotectonic fault at the western slope of Mt Vettore, triggered by the 26-30/10/2016 earthquakes. The photos and models were used to map in detail rupture zones in specific sites of interest, as well as to identify subtle morphological features possibly associated with the faults in question. The total length of surveyed surface ruptures showing evidence of primary surface faulting along the Mt. Vettore fault is at least 5 km, with a reactivation of the northern part of the “Cordone del Vettore” fault trace. Whereas in the Castelluccio basin there is a NNE-SSW trending ground fracture displayed just south of the village of Castelluccio.



Fig.6. The ground ruptures observed on the elluvium cropping out on the southern slope of Mt. Vettoretto.



Fig.7. Left: The normal component of the co-seismic fault reactivation. Right: co-seismic displacement on the bedrock (limestone) after the August earthquakes.



Fig.8. Co-seismic fault traces after the October 2016 seismic activity.



Fig.9. Co-seismic displacement on the Vettore fault after the October 2016 of more than 50 cm

3. Earthquake's secondary ground deformation

Numerous observed and mapped rock falls, slides of earth-materials etc. (Fig. 10), occur mainly along the high-relief area of the footwall, the mountain roads and on artificial slopes. They were studied with preliminary mapping from satellite imagery, and examples are presented of large landslides in the epicentral region with pre- and after-the earthquake images.

The main source for landslide mapping were Sentinel-2A images (from Copernicus Science Hub, ESA) with a pixel size of 10 m. Additional info for the landslides of the August 24 event were collected from a Rapideye (5 m) image (20170825 ©2016 Planet Labs). A total number of 162 sizeable (5 – 10 m) landslides were identified for the whole sequence (Fig. 11). The majority of landslides mapped were formed during the 1st event (August 24). This is believed to be associated with the large landslides being near their critical state, which was surpassed by the strong ground motion of the 1st Mw 6.2 earthquake. The total number of landslides (162) is smaller than the number (811 for the whole earthquake sequence) released by the Italian catalogue of earthquake-induced ground failures CEDIT (Fortunato et al., 2012; Martino et al., 2016) but the difference is attributed to the inability of high-resolution satellite imagery used (5 – 10 m) to identify smaller landslides or rock falls.



Fig.10. Field photos of rock falls in the area around Mt Vettore after the August earthquakes.

From the radar interferometry results of ALOS-2 (GSI, 2016) and Sentinel-1 (Copernicus Sentinel data, 2016; Marinkovic and Larsen, 2016), a number of 20 large unstable areas was identified (Fig. 11). These show a deformation of 4-10 cm and are interpreted as bed-parallel slip or slow moving deep-seated landslides that are activated by the 2016 earthquakes. Although these lack any surface expression, the movement detected by radar interferometry indicates passive re-activation during the earthquake events. The 162 mapped landslides are distributed in an area of up to 30 km from epicentre/surface rupture, with the majority being at 10 km or less from the surface ruptures. Comparing the mapped landslides with the Italian landslide inventory (*Inventario dei Fenomeni Franosi in Italia*, IFFI project, ISPRA – Dipartimento Difesa del Suolo Servizio Geologico d' Italia, available at: <http://www.progettoiffi.isprambiente.it>), the new landslides are mostly within near-field range of the surface ruptures, while far-field landslides are cited in pre-existing landslide prone areas. This means that the earthquake was strong enough to create new surface phenomena, while also being a triggering factor to already landslide prone areas further away.

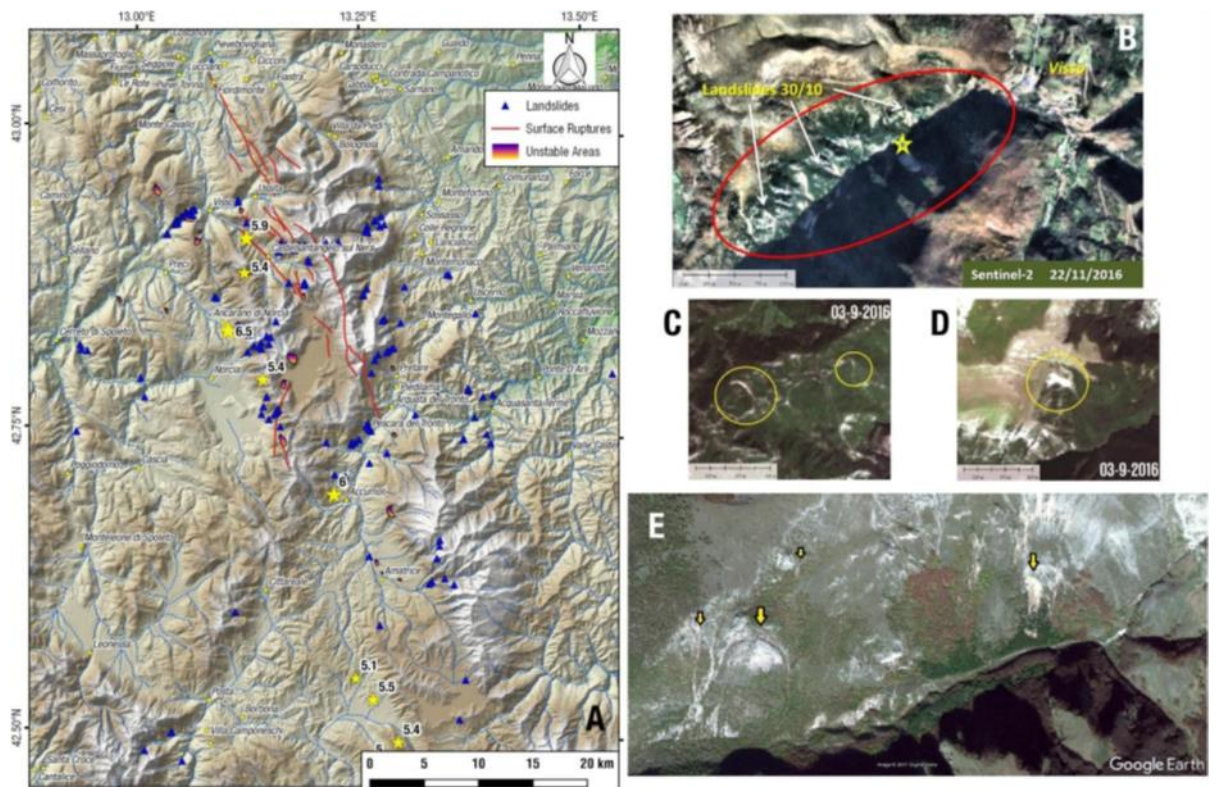


Fig.11. A) Landslides mapped using satellite imagery and InSAR, for the 2016 earthquake sequence. B) Sentinel-2A image of landslides near Visso from the Oct.30 event. Star shows the large landslide that dammed Nera river. C & D) Landslides from the Aug.24 event. (Sentinel-2A). E) Landslides NE of Norcia originated from the Oct. 30 event (Google Earth image, 31/10/2016).

4. Fault modelling

The correlation between seismic sources and the five major earthquakes of the sequence is shown below:

24/08/2016, 01:36:32.3 GMT (1st shock), Mw 6.2, Seismic source F1
 24/08/2016, 02:33:29.4 GMT (2nd shock), Mw 5.6, Seismic source F2
 26/10/2016, 17:10:36.2 GMT (1st shock), Mw 5.5, Seismic source F3
 26/10/2016, 19:18:07.2 GMT (2nd shock), Mw 6.1, Seismic source F4
 30/10/2016, 06:40:18.3 GMT, Mw 6.6, Seismic source F5

The basic philosophy for modelling the seismic sources is based on the Individual Seismogenic Sources (ISS) of DISS (Basili et al., 2008). Although most of the parameters are geologically, seismologically or even geodetically constrained, source dimensions sometimes cannot be directly defined. For this reason, the following scaling relationships between seismic moment, moment magnitude and fault plane dimensions were used (Aki, 1966; Hanks and Kanamori, 1979; Wells and Coppersmith, 1994), either combined or stand-alone, depending on the available data:

$M_0 = \mu \cdot u \cdot L \cdot W$ (Aki, 1966), where M_0 is moment, μ is shear modulus, u is average slip, L is length and W is width

$M_w = 1.54 \cdot \log L + 4.34$ (Wells and Coppersmith, 1994), for calculating length (L) from M_w for normal faults,

$M_w = 2.11 \log W + 4.04$ (Wells and Coppersmith, 1994), for calculating downdip width (W) from M_w for normal faults,

$M_w = 0.82 \cdot \log (L \cdot W) - 2.87$ (Wells and Coppersmith, 1994), for calculating either length (L) or width (W) from M_w for normal faults, and

$M_w = \frac{2}{3} \cdot \log M_0 - 10.7$ (Hanks and Kanamori, 1979)

The modelling of the seismic sources is illustrated in Fig. 12 and their parameters are listed in Table 2.

4a. The August 24 earthquakes (seismic sources F1 and F2)

Both strongest events on August 24, the first of Mw 6.2 and the second of Mw 5.6, were produced by two respective, almost pure normal, WSW- to SW-dipping faults suggested from both focal mechanisms (Table 1) and our field observations (Fig. 12). According to INGV, the first earthquake occurred more than 2 km WNW of Accumoli and the second one in a distance 11.5 km to the NW, ca. 5 km east of Norcia. The fault system has a clear morphological expression dipping to the WSW along the Gorzano

and Vettore mountain-fronts which was already mapped in previous studies (e.g. Calamita & Pizzi, 1992; 1994; Calamita et al., 1992; 1994; Centamore et al., 1992; Galadini & Galli, 2000; Boncio et al., 2004; Pizzi & Galadini, 2009) and published geodatabases (DISS Working Group, 2015; ITHACA, 2000). Both events induced a variety of secondary ground deformation phenomena, such as ground ruptures, rockfalls and landslides (e.g. EMERGEO W.G., 2016; Pavlides et al., 2016).

Table 2: The basic parameters of the five seismic sources (Fig. 12).

Fault #	Length (km)	Down-dip Width (km)	Minimum Depth (km)	Maximum Depth (km)	Strike (°)	Dip (°)	Rake (°)	Average slip (m)
F1	16.0	10.0	5.0	12.5	165	49	-78	0.45
F2	9.0	13.0	0.5	9.5	143	44	-82	0.08
F3	8.0	8.0	5.0	9.9	161	38	-90	0.11
F4	18.0	13.0	0	10.0	155	50	-89	0.24
F5	25.0	15.0	0	10.4	152	44	-94	0.71

However, we observed coseismic ground ruptures for a total length of ca. 8 km only along the Vettore mountain-front, close to the epicentral area of the second strongest event which is in agreement with other observations as well (EMERGEO W.G., 2016a; 2016b; Binda et al., 2016; Blumetti et al., 2016; Piccardi et al., 2016; Livio et al., 2016; Aringoli et al., 2016). Although there is an open debate about whether these ruptures are primary or secondary effects (e.g. landsliding and sediment compaction due to ground shaking) (Gruppo di Lavoro IREA & INGV, 2016), we clearly observed offset on basement rocks bearing bands of the latest activity on the free faces, thus suggesting surface emerging fault rupture. The locations of both coseismic ruptures and epicentres imply that ruptures were produced only by the second smaller event (seismic source F2). The length of these ruptures was used to constrain the minimum length of seismic source F2.

The lack of co-seismic ground ruptures along the seismic source F1 suggests that rupture propagation of the latter was constrained at depth. Aftershock vertical distribution of the first shock was mostly concentrated between depths of 5 and 13 km, whereas a major cluster is depicted in the vertical distribution of the second shock, reaching a maximum depth of ca. 12-13 km (INGV's preliminary catalogue; Michele et al., 2016).

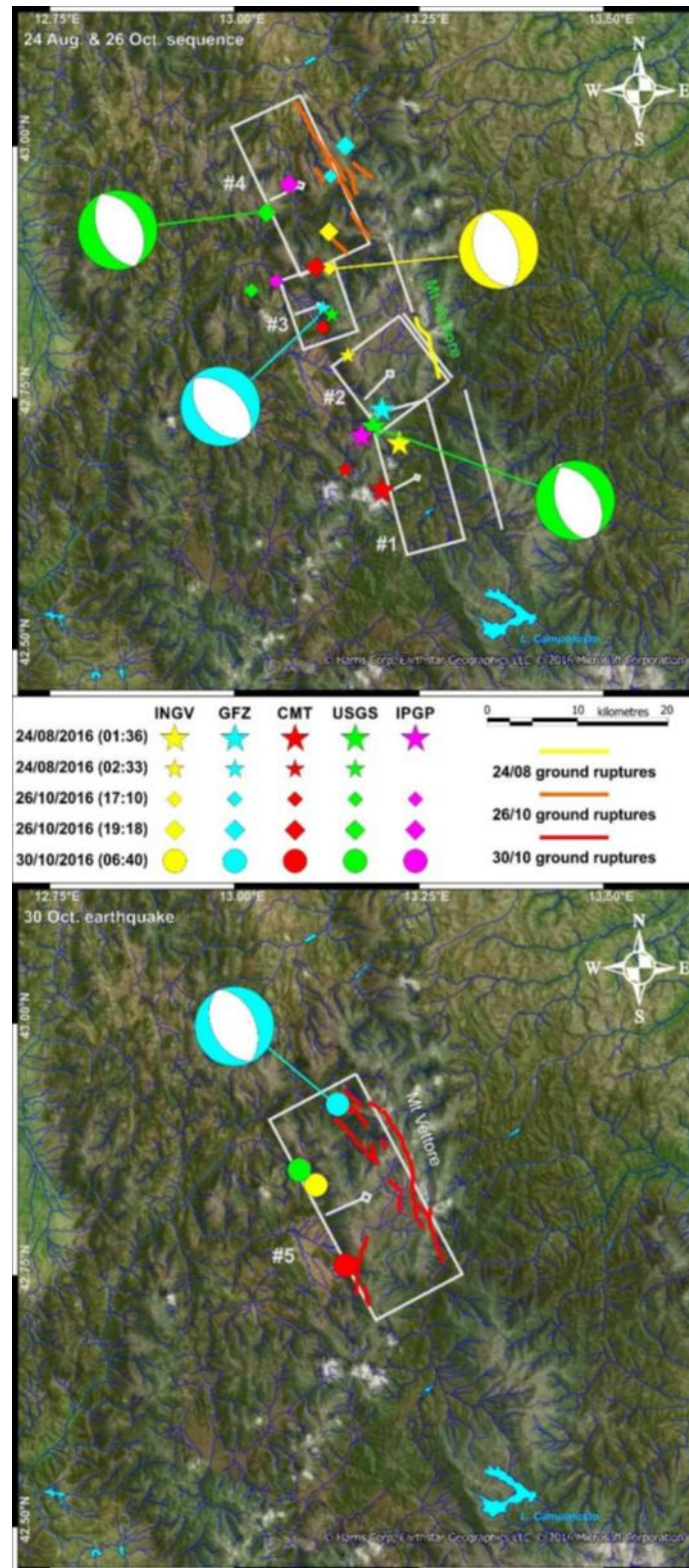


Fig.12. The five groups of epicentres and the seismic sources (see Table 2 for the parameters) corresponding to the strongest events of the 2016 seismic crisis in Central Italy (August 24 and October 26 on top and October 30 at the bottom). The focal mechanisms used for geometric and kinematic attributes are also shown.

The dimensions of seismic source F1 were estimated from the empirical relationships of Wells and Coppersmith (1994). Considering the mapped fault scarp at the northwestern mountain-front of Mt Gorzano, we preferred to obtain the geometric and kinematic attributes of the seismic source from the focal mechanism of USGS. Keeping in mind the maximum depth of the aftershock distribution, the calculated dimensions and the dip angle from the focal mechanism, we calculated a minimum depth of 5 km for the fault plane. Average slip was derived from M_0 , M_w and the source dimensions after applying the formula of Aki (1966).

The definition of the dimensions and position of seismic source F2 is less straightforward. The two direct limits of the fault plane are the extent of the surficial ruptures (a minimum length of 8 km) and the depth of the aftershock cluster (a maximum depth of 10-11 km). The focal mechanism that best matches the geological observations is the one of GFZ (Table 1, Fig. 11), which suggests a fault dip of 44° . Considering all the above constraints, we set the dimensions of the fault plane to 9×13 km (length \times width, respectively) extending between the depths of 0.5 and 9.5 km (minimum and maximum respectively). The 0.5 km value of minimum depth aims to indicate that the rupture partially reached the surface. To retain the seismic moment at the order of ca. $3.0E+17$ N-m the average slip had to be reduced to 0.08 m according to Aki's (1966) relationship.

4b. The October 26 earthquakes (seismic sources F3 and F4)

Almost two months later, on October 26, a moderate (M_w 5.5) and a strong (M_w 6.1) earthquake stroke the same area, northern from the previous two events, rupturing two adjacent fault segments, F3 and F4, respectively (Fig. 12). Based on the ca. 17 km-long co-seismic ground ruptures along the western mountain-front of Mt Vettore from our field observations (for seismic source F4), previous works (e.g. Calamita & Pizzi, 1992; 1994; Calamita et al., 1992; 1994; Centamore et al., 1992; Blumetti et al., 1993; Galadini & Galli, 2000; Borre et al., 2003; Pizzi & Galadini, 2009) and published geodatabases (Basili et al., 2008; ITHACA, 2000), we preferred the focal mechanisms of INGV and USGS (Table 1; Fig. 12) for the geometric and kinematic attributes of seismic sources F3 and F4, respectively. We should mention that no co-seismic ground ruptures were associated to the first event (source F3), implying a blind fault plane. A cluster that can be detected in the aftershock vertical distribution of the first shock (INGV's preliminary catalogue; Michele et al., 2016) extends between the depths of approximately 5 and 10 km. Taking under consideration the fault dip taken from the respective focal mechanism, we estimated F3's down-dip width to 8 km. The

length of 8 km was calculated from the M_w versus subsurface rupture length empirical relationship of Wells and Coppersmith (1994). In order not to exceed the seismic moment of $1.5\text{-}2.5\text{E}+17$ N-m with such large dimensions in Aki's (1966) formula, an average seismic slip of 0.11 m was set. Concerning source F4, its 18-km length was constrained by the extent of the ground ruptures and its 13 km down-dip width by the approximately 11 km depth of the aftershock cluster (INGV's preliminary catalogue; Michele et al., 2016). As in the previous case, average slip was set to 0.24 m so as not to exceed the seismic moment.

4c. The October 30 earthquake (seismic source F5)

The strongest shock of the whole sequence, the October 30 (M_w 6.6) event, is a clear case of fault linkage: during the event, both fault segments F2 and F3 were totally re-ruptured as suggested by i) the proposed epicentres of the mainshock and the aftershock horizontal distribution, ii) the co-seismic ground ruptures, and iii) the deformation pattern of InSAR images. Based on fault dimensions (25 km length and 15 km width) estimated by the relationships of Wells & Coppersmith (1994) and constrained by the co-seismic ground ruptures, it is obvious that seismic source F5 not only fully breached these two segments, but it also partially re-ruptured source F4 and possibly a small portion of source F1. The extended occurrence of ground ruptures clearly indicates an emerged source. Depth was constrained not only from the sources geometrical features, but from the hypocentral distribution of both mainshock and aftershocks (Michele et al., 2016). The focal mechanism of GFZ is the one that better describes the strike of the co-seismic ground ruptures. (Fig. 12).

5. Ground deformation pattern

Our modelled seismic sources were used to calculate the cumulative ground deformation pattern after each main event of the sequence by applying the Okada (1992) dislocation solution formulae for a homogeneous, elastic and isotropic half-space, through the Coulomb v3.3 application (Toda et al., 2005). We will also compare our theoretical results with various published interferometric images, such as ALOS-2 (GSI, 2016) and Sentinel-1 (Copernicus Sentinel data, 2016; Marinkovic and Larsen, 2016).

a. The deformation of August 24 earthquakes (source faults F1 and F2 respectively)

The first dislocation model reflects the cumulative ground deformation caused by the two strongest shocks on August 24, corresponding to faults F1 and F2 respectively (Fig. 13a, b and c). As expected from the faults' kinematics, the most significant

component is the vertical displacement, the maximum value of which is calculated at ~14 cm. The InSAR images that best describe the deformation of the August 24 events derive from the ALOS-2 (23.6 cm wavelength; 13d) and Sentinel-1 (5.56 cm wavelength; 13e and f) satellite sensors. The narrowest time envelope belongs to the Sentinel-1 images which were acquired 3 days before and after the events (21/8/2016 – 27/8/2016).

b. *The deformation of October 26 earthquakes (source faults F3 and F4 respectively).*

The second dislocation model involves the cumulative ground deformation induced by the two strongest shocks on October 26, corresponding to faults F3 and F4 respectively (Fig. 14a, b and c). As in previous case, the most significant displacement component is the vertical, the maximum value of which is calculated at ~15 cm. The interferogram of the Sentinel-1 satellite sensor (5.56 cm wavelength; Fig. 14d) is the one that chronologically bounds these two events, with the two images acquired 11 days before and 1 day after the events (15/10/2016 – 27/10/2016, respectively).

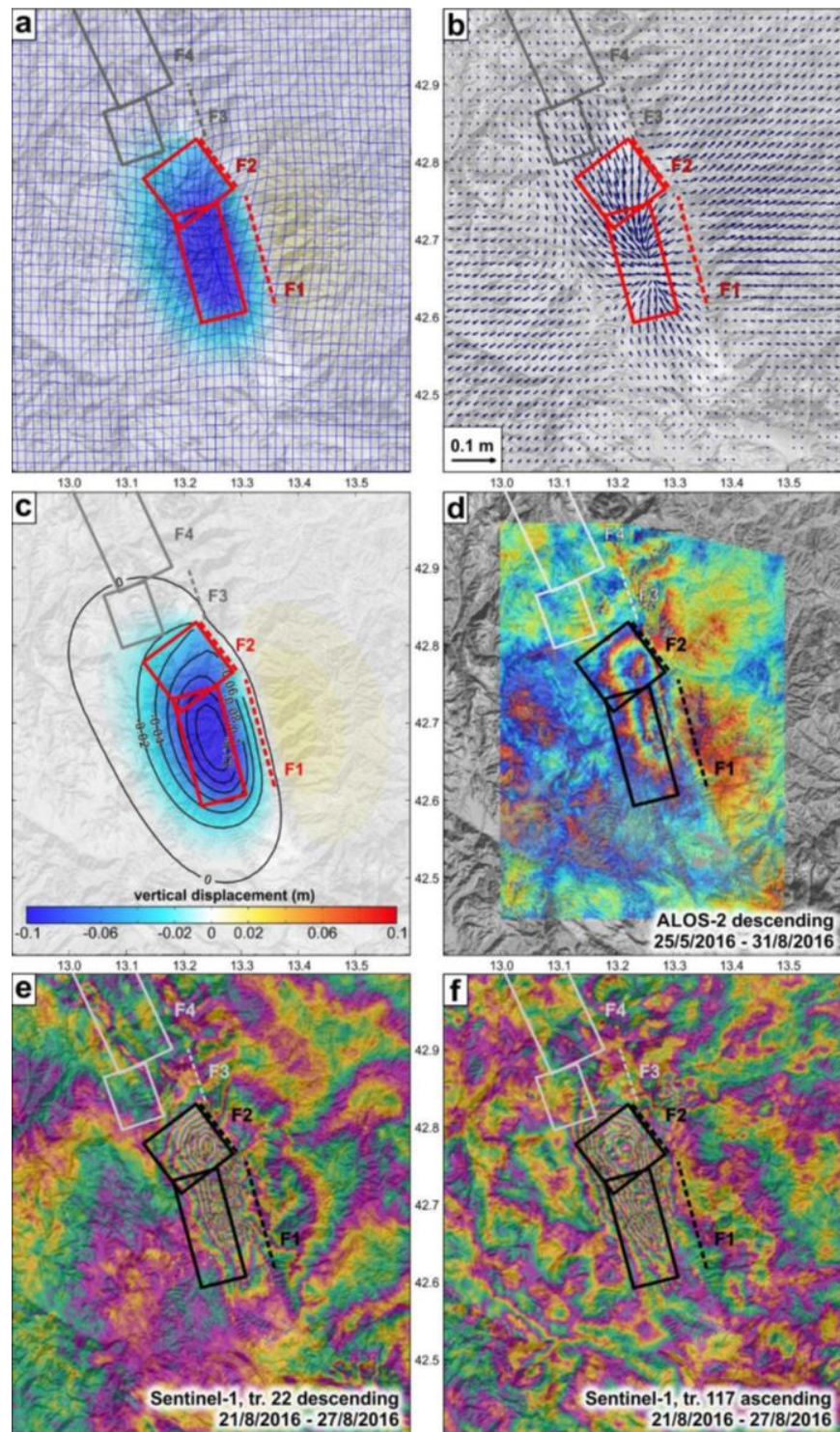


Fig.13. Theoretical dislocation model on ground depth showing (a) combined horizontal and vertical, (b) horizontal, and (c) vertical displacements after the reactivation of seismic sources F1 and F2. InSAR images, which envelop the two strongest events on August 24, acquired from: (d) ALOS-2 sensor (descending orbit) for a time window between 25/5/2016 and 31/8/2016 (GSI, 2016), (e) Sentinel-1 sensor (descending orbit) for a time window between 21/8/2016 and 27/8/2016, and (f) Sentinel-1 sensor (ascending orbit) for a time window between 21/8/2016 and 27/8/2016 (Copernicus Sentinel data, 2016; Marinkovic and Larsen, 2016). The seismic sources are superimposed.

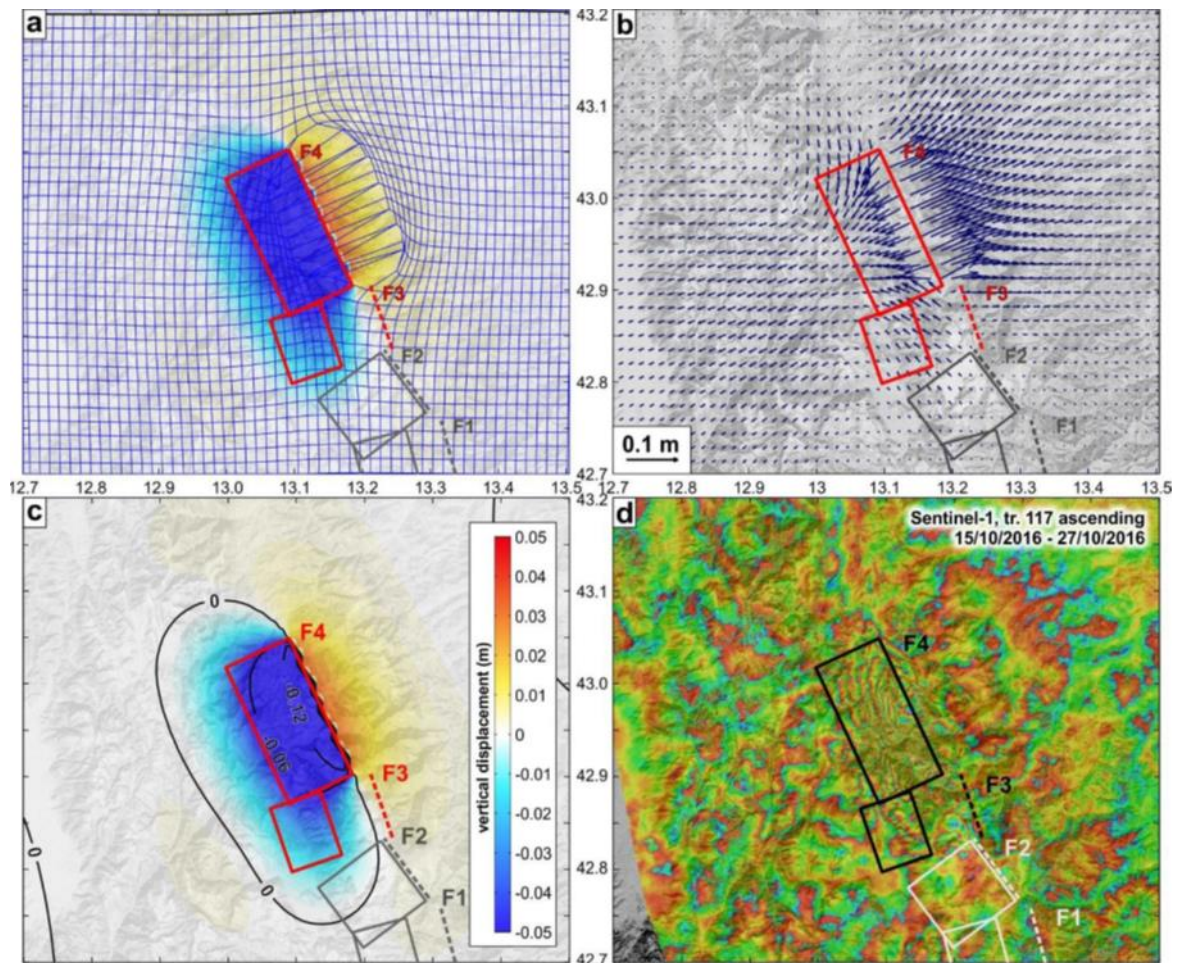


Fig.14. Theoretical dislocation model on ground depth showing (a) combined horizontal and vertical, (b) horizontal, and (c) vertical displacements after the reactivation of seismic sources F3 and F4. (d) InSAR image, which envelops the two strongest events on October 26, acquired from the Sentinel-1 sensor (ascending orbit) for a time window between 15/10/2016 and 27/10/2016 (Copernicus Sentinel data, 2016; Marinkovic and Larsen, 2016). The seismic sources are superimposed.

c. The deformation of August 24 and October 26 earthquakes (source faults F1, F2, F3 and F4 respectively)

The cumulative ground deformation pattern of the four strongest shocks on August 24 and October 26, corresponding to faults F1-F4, respectively, is shown in Fig. 15a, b and c. The maximum vertical displacement is calculated at ~15 cm. The interferogram that covers this time period is the ALOS-2 (23.6 cm wavelength; 15d). However, the time span of the acquired images is quite long creating a large gap of more than 6 months before the first events on August 24 (5/2/2016). The second image was taken 2 days after the last event of October 26 (28/10/2016).

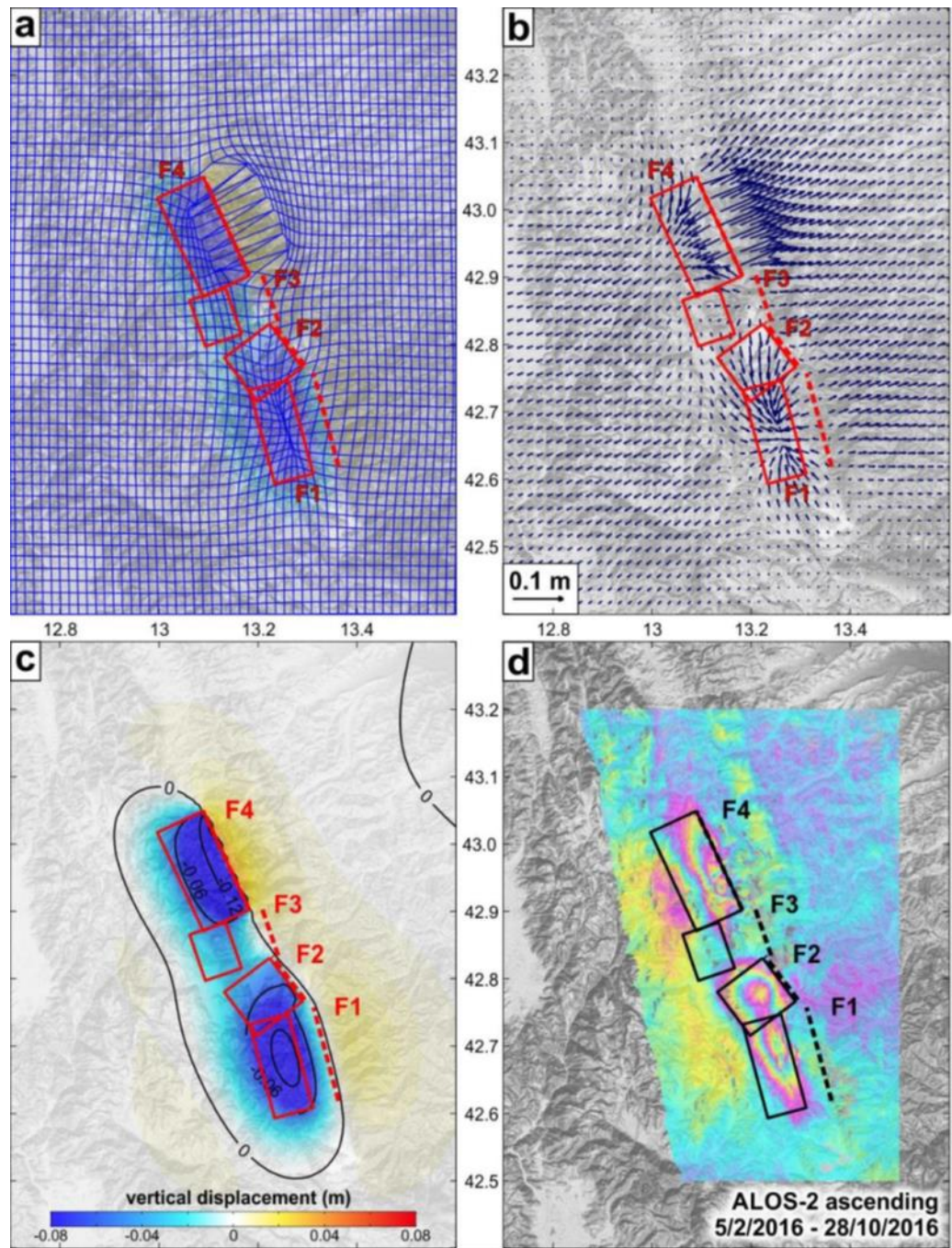


Fig.15. Theoretical dislocation model on ground depth showing (a) combined horizontal and vertical, (b) horizontal, and (c) vertical displacements after the reactivation of seismic sources F1, F2, F3 and F4. (d) InSAR image, which envelopes the four strongest events on August 24 and October 26 respectively, acquired from the ALOS-2 sensor (descending orbit) for a time window between 5/2/2016 and 28/10/2016 (GSI, 2016). The seismic sources are superimposed.

d. The deformation of October 30 earthquake (source fault F5)

The ground deformation pattern of the October 30 strong shock (corresponding to fault F5) is shown in Fig. 16a, b and c. The maximum vertical displacement is calculated at ~41 cm. Concerning interferometry, there was a very narrow time window for the first image to be acquired (between 26/10 and 30/10); nevertheless, interferograms from

both ALOS-2 (23.6 cm wavelength; 16d) and Sentinel-1 (5.56 cm wavelength; Fig. 5e) satellite sensors were able to isolate this particular event. The former has a time span between 28/10/2016 and 11/11/2016 and the latter between 27/10/2016 and 2/11/2016.

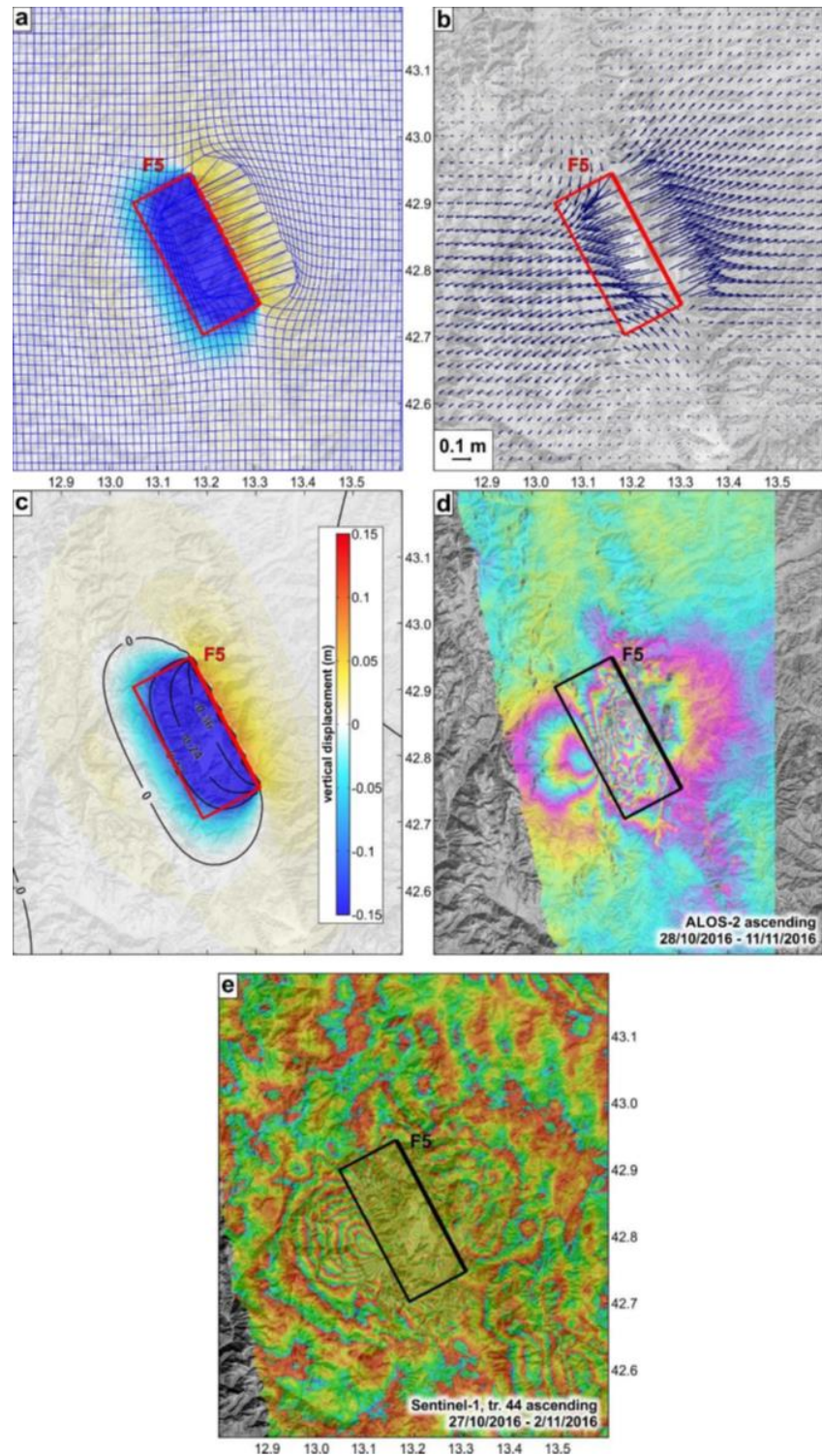


Fig.16. Theoretical dislocation model on ground depth showing (a) combined horizontal and vertical, (b) horizontal, and (c) vertical displacements after the reactivation of seismic source F5. InSAR images, which envelop the strong event on October 30, acquired from: (d) ALOS-2 sensor (ascending

orbit) for a time window between 28/10/2016 and 11/11/2016 (GSI, 2016), and (e) Sentinel-1 sensor (ascending orbit) for a time window between 27/10/2016 and 2/11/2016 (Copernicus Sentinel data, 2016; Marinkovic and Larsen, 2016). The seismic sources are superimposed.

After comparing the seismic sources and their modelled deformation with the interferograms, we reached to the following conclusions: at first, the position of all seismic sources is in accordance with the shape of the fringes in all interferograms. Furthermore, our modelled deformation patterns resemble very well the deformation calculated in the interferograms. Concerning the two main events on October 26 (Fig. 14 and 15), there is an obvious abrupt change of the fringes' shape at the southern tip of seismic source F4 that leads to an absence of deformation along seismic source F3, confirming the fact that source F3 is indeed blind. The maximum vertical displacement in all our models is at the same order of magnitude and close to the respective displacements observed in the InSAR images. Small values depreciation can be considered logical given that i) our displacement model concerns a homogeneous, elastic and isotropic half-space, while InSAR images include deformation also induced by observed secondary effects such as ground compaction and deep seated gravitational slides (Aringoli et al., 2016; Huang et al., 2017), and ii) the InSAR image involves not only the deformation of the mainshocks, but the cumulative deformation produced by the aftershock activity as well.

6. Discussion and Conclusions

6.1 Static stress changes

When an earthquake occurs, the average stress on the fault that slipped is reduced, while stress is increased at the tips of its plane and at sites around it, causing stress to increase or decrease at other faults, and thereby advance in time or delay the earthquake occurrence on them (e.g. Reasenberg and Simpson, 1992; King et al., 1994; Hodgkinson et al., 1996; Zhang et al., 2003). Accumulation or release of stress on a fault is controlled not only by the regional stress field and rock property, but also by its surrounding faults. For a fault to slip, Coulomb stress change $\Delta\sigma_f$ should exceed a threshold value on its plane:

$$\Delta\sigma_f = \Delta\tau_s + \mu' \cdot \Delta\sigma_n$$

where $\Delta\tau_s$ is the shear stress change on the failure plane, μ' is the friction coefficient and $\Delta\sigma_n$ is the normal stress change. Stress change distribution is calculated by the Coulomb v3.3 application (Toda et al., 2005) which resolves the shear and normal components of the stress change on a grid or on specified 'receiver' fault planes, in a homogeneous, elastic and isotropic half-space. According to Toda et al. (2011), "source

faults” are the faults that have slipped and “receiver faults” are planes with a specified strike, dip and rake, on which the stresses imparted by the source faults. Thus, shear stress change is dependent on the position, geometry, and slip of the source fault and on the position and geometry of the receiver fault, including its rake, whilst normal stress change (clamping or unclamping) is independent of the receiver fault rake.

a. Post-sequence scenarios

Our aim is to calculate the post-sequence Coulomb stress change for the (receiver) faults in the surrounding area after the total rupturing of all five seismic sources (F1, F2, F3, F4 and F5). Based on their attributes, receiver faults in the area (Fig. 17) (Calamita & Pizzi, 1992; 1994; Calamita et al., 1992; 1994; Centamore et al., 1992; Blumetti et al., 1993; Boncio & Lavecchia, 2000; Galadini & Galli, 2000; 2003; ITHACA, 2000; Pizzi et al., 2002; Borre et al., 2003; Tondi & Cello, 2003; Boncio et al., 2004; Roberts & Michetti, 2004; Galli et al., 2005; Pace et al., 2006; Pizzi & Galadini, 2009; Walker et al., 2012; DISS Working Group, 2015) can be separated into two groups: Group A (faults in red colour, Fig. 17) consists of NNW-striking faults similar to our modelled seismic sources. These faults demonstrate normal kinematics and moderate dipping angle as suggested by focal mechanisms of the recent sequence (from both mainshocks and selected aftershocks), the September-October 1997, Colfiorito sequence and the sparse microseismicity (e.g. RCMT catalogue). Dip direction is not important for the stress change distribution. Thus, the characteristic parametric values attributed to this fault group are: strike = 155° , dip = 45° and rake = $27-90^\circ$.

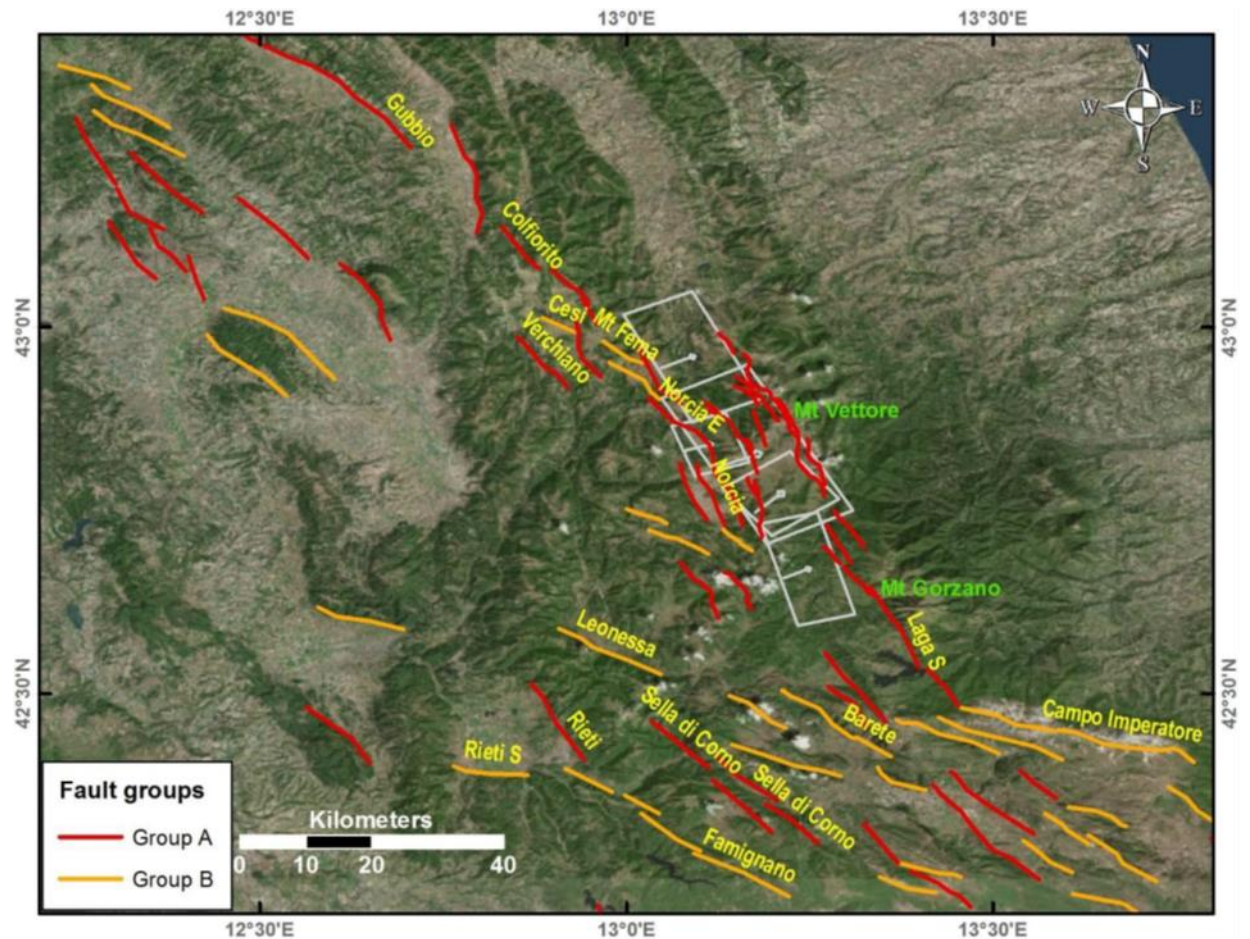


Fig.17. Neotectonic map of the broader study area. Faults are separated into two groups based on their attributes (see main text for details). The five seismic sources of the 2016 are also shown in white. For faults references see main text.

Group B (faults in amber colour, Fig. 17) consists of NW- to WNW-striking faults, mainly observed east from the Lake Campotosto, as the “Campotosto Lake-Montesilvano” CSS (ITCS075) in DISS (DISS Working Group, 2015) or the broader “Faglia delle Tre Selle” - “Campo Imperatore” fault zone in ITHACA (2000). In DISS this CSS is described as “a long strike-slip (to oblique), right-lateral fault system that is thought to run ca. E-W across the northernmost sector of the Apulian domain”. In fact, the associated “Isola del Gran Sasso” ISS (ITIS096) near to the Lake Campotosto can be used as a representative seismic source of this fault group, with the following parameters: strike = 095° , dip = 75° and rake = -135° .

Three indicative calculation depths (4, 8 and 12 km) are selected for each fault group, according to the regionally inferred maximum fault depths and hypocentral depths of the mainshocks. Results for receiver faults as in Group A (Fig. 18) show that stress rises at all depths along the strike direction of the seismic sources, including the Colfiorito fault zone to the north and the Laga S. and Capitignano fault zones to the south (Fig. 17). It is noteworthy that for the shallow depth of 4 km, stress rises

significantly above seismic source F1 and for all depths above 5 km (where the upper tip of F1 is located). However, the largest part of the affected area demonstrates stress drop along a NE-SW-trending transverse zone (relative to the faults' strike), including the faults directly located at the footwall or hanging-wall of the source faults. Only at the depth of 12 km (the lowest parts of the faults) stress increases near to the deepest edge of the source faults. Similar results are shown for faults of Group B (Fig. 18) with a slight counter-clockwise distortion: stress increase is mainly concentrated in a more WNW and ESE direction at the NW and SE tips of the source faults system, respectively, whereas stress decrease is widely spread in a more NNE-SSW direction. The Cesi Fault, at the hanging-wall of F4 (see also 17), shows stress load at all depths. The adjacent Mt Fema Fault demonstrates a variable stress change: stress increases at shallow and great depths (horizontal sections 4 and 12 km, respectively in Fig. 18) and decreases around the depth of 8 km (Fig. 18). The westernmost segments of the broader "Campo Imperatore" (ITHACA, 2000) or else "Campotosto Lake-Montesilvano" CSS (DISS Working Group, 2015) shows a small amount of stress load. All faults of Group B located at the hanging-wall of the source faults, such as the Leonessa Fault (see also Fig. 17), are in a state of stress relief at all depths. Like for Group A, a similar stress increase is observed at shallow depths above the upper part of seismic source F1; however only faults of Group A are met in this narrow zone.

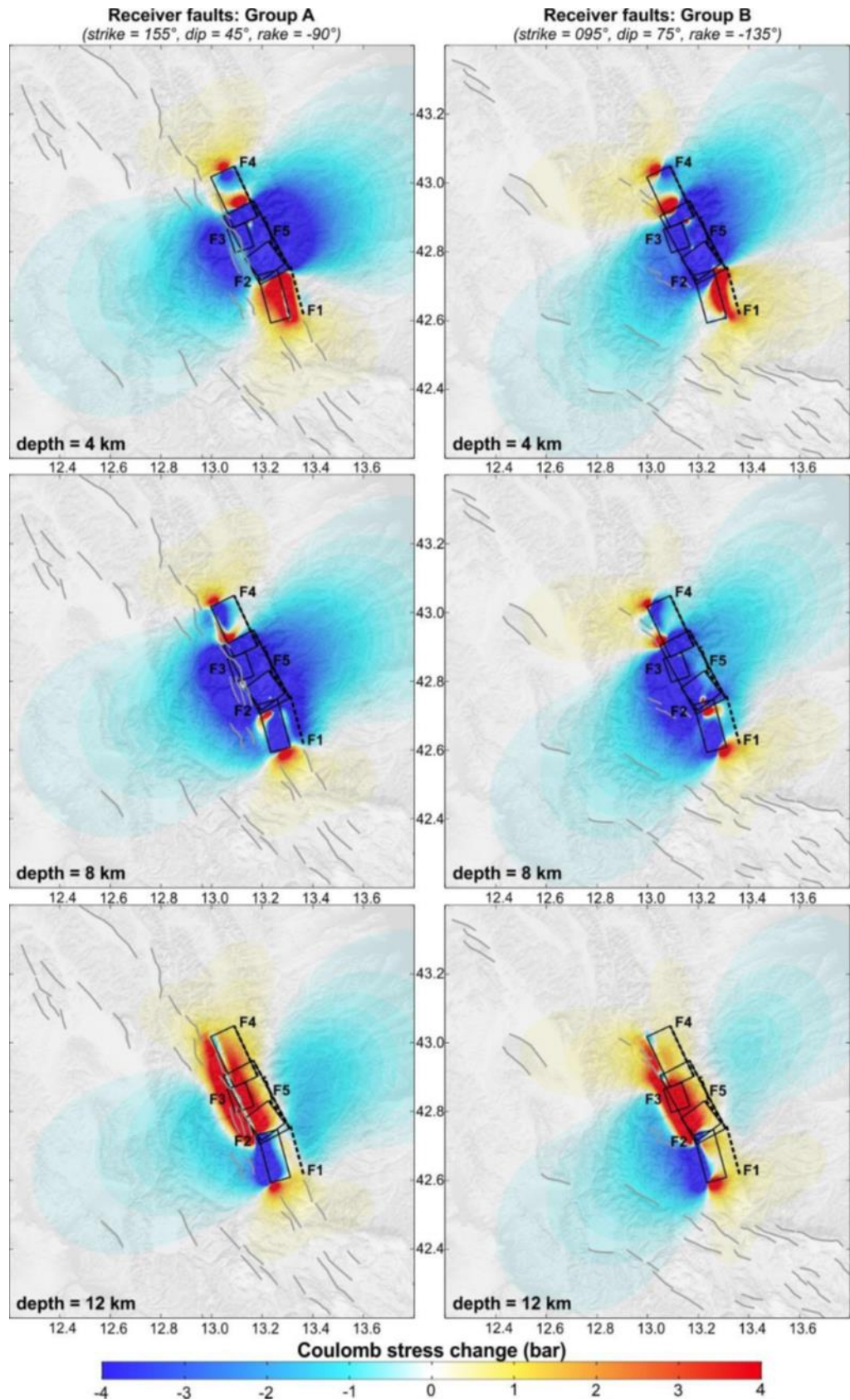


Fig.18. Coulomb stress change patterns at the depths of 4, 8 and 12 km after the rupturing of the five seismic sources that caused the five strongest shocks during the 2016 seismic crisis in Central Apennines. The method was applied for the two fault groups, Group A and B, recognised in the surrounding area (see text for details and references).

6.2 Campotosto aftershocks of January 2017

In January 18 2017, four events of magnitude greater than 5 occurred immediately SW of the F1 seismic source (Fig.19). Based on their epicentres located in the highly stress load area, the epicentral depths of maximum 12 km and the proposed WSW-dipping, normal nodal planes (as in Group A), it is clear that they were triggered by the reactivation of the five seismic sources of the August-October sequence. Deformation observed in interferograms published by IREA-CNR & INGV (2017) show a maximum subsidence of ~10cm to the NW of Lake Campotosto (Fig. 19), indicating a fault rupture along the central part of Laga Fault plane. As described in the previous chapter, the area of the January aftershocks is inside a positive stress loading area, also confirmed by Papadopoulos et al. (2017). This is interpreted as one or more patches on Laga Fault that did not rupture during the August 24 event and a possible southern limit of August 24 fault plane rupture. It is worth noting that the rest part of the southern segment of Laga Fault, south of Campotosto Lake was ruptured during the April 9, 2009 Mw 5.2 aftershock of the L'Aquila earthquake sequence, with a displacement of ~20cm at depth (Cheloni et al., 2014). The January 18 rupture fills the gap between the 2009 Campotosto and the August 24 Amatrice events, completing the rupture along a ~70km long stretch of Mt Vettore and Laga faults.

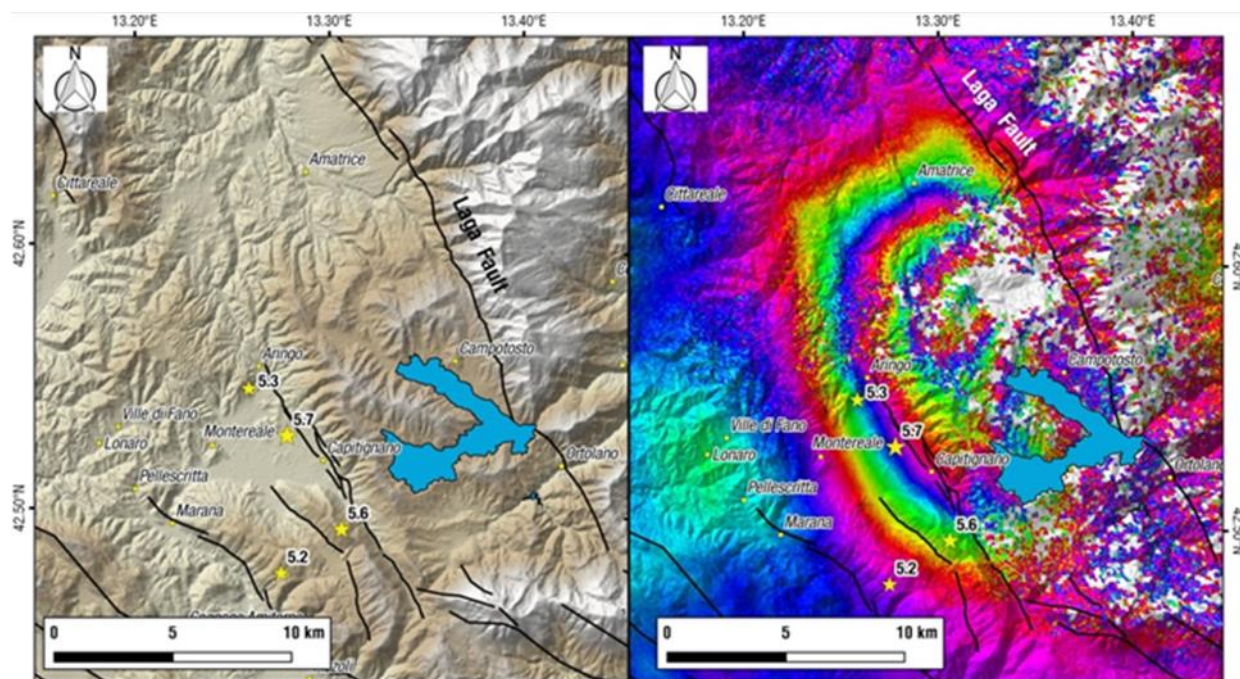


Fig.19. Left: The January 18 2017 earthquake cluster near Lake Campotosto. Stars mark epicenters and magnitude (M_w), in relation to the southern part Laga fault. Right: Interferogram between 2016/12/13 & 2017/02/11 from IREA-CNR & INGV (2017). Fringes indicate rupture that correlates with the west dipping Laga fault plane.

Concerning historical seismicity, there is a complete absence of earthquakes along the southern part of Laga fault from the Middle-Ages up to the 2009 Campotosto earthquake (Galli et al., 2017). The northern segment of Laga fault, east of Amatrice, is associated only with the 1639 event (Boncio et al., 2004, Galli et al., 2017), an earthquake partly overlapping with the 2016 earthquakes. This is an important observation concerning seismic hazard in the area, since a complete rupture of the Laga fault is not supported by historical and instrumental observations. Apart from the northern segment near Amatrice and Accumoli, the southern/central smaller segments of the fault are activated mainly in small/moderate earthquakes and aftershocks of nearby events, with small displacements.

6.3 Conclusions

The August-October 2016 seismic crises consisted of a complex succession of five moderate-to-strong earthquakes and involved fault linkage and possible earthquake triggering effects. The successive fault reactivation motivated us to calculate the post-sequence static stress change for adjacent faults in the surrounding area. The faults responsible for the five major events were modelled based on available information such as geological, seismological and geodetic data. The four seismic sources (F1-F4) of the respective first four major events are aligned along strike in a NNW-SSE general direction, dipping to the WSW (Fig. 11, top). Seismic sources F1 and F3 are blind as it is evident from the lack of co-seismic primary ground ruptures. During the fifth event (October 30), seismic sources F2 and F3 were breached, with the rupture expanding not only horizontally (by re-rupturing a significant part of F4 and a small part of F1), but also vertically (from the maximum depth of ca. 10 km up to the surface). This event is represented by seismic source F5.

The five seismic sources were used to calculate the ground deformation based on the Okada (1992) model. The modelled deformation was compared with InSAR images to confirm our fault models. In our given example (Fig. 4), we used the first four seismic sources (F1-F4) corresponding to the four events on August 24 and October 26, and we compared their deformation with the ALOS-2 InSAR image for the period between February 5 and October 28, 2016. The modelled deformation pattern agrees with the InSAR image and the maximum subsidence is calculated at ~15 cm, while in the InSAR image is measured at ~25 cm. The results are quite satisfactory giving confidence to our models.

The post-sequence Coulomb static stress changes were calculated for the surrounding faults, setting as source-faults all five seismic sources (F1-F5). Receiver faults were obtained from mapped and studied faults from other published works for the broader area. According to their main attributes (strike, dip and rake), the surrounding faults were divided into Group A, which includes NNW-SSE-striking normal faults with moderate dip angles (similar to the source-faults), and Group B, which includes WNW-ESE-striking, oblique to dextral strike-slip faults with steeper dip angles. Group A shows stress load on neighbouring faults that are located bilaterally along the source-faults' strike. In contrast, faults located in the footwall or hanging-wall of the source-faults are relieved from stress. However, at the depth of 12 km stress increases near to the deeper parts of F4 and F5 (including F2, F3) favouring triggering for parallel antithetic faults. This group also includes the adjacent Colfiorito fault zone, which was reactivated in 1997, but did not produce any significant event during the 2016 sequence. Possibly, the 1997 sequence significantly relieved stresses on the Colfiorito fault plane and the 2016 sequence did not intensify them enough to trigger it. Group B shows an almost similar stress change pattern. In fact, the western fault segments of the "Campotosto Lake-Montesilvano" CSS (DISS Working Group, 2015) are lightly loaded at all depths. For the receiver faults located towards the hanging-wall of the five source-faults stress drops. In conclusion, Coulomb stress change results suggest that further earthquake triggering is very possible in relatively close distances beyond the along-strike tips of the fault system, as is also proved by the very recent activity on January 18, 2017. However, stress drop occupies a larger part of the surrounding area.

The earthquake sequence of August-October 2016 has some special characteristics different from previous earthquakes either in Apennines or elsewhere, such as widespread co-seismic fractures and pair ("double") events, that is quadruplicate seismic activity and the fifth stronger event re-activating more or less the same fault segments. The surficial and, especially, the deeper geometry of the fault structures are much complex, following the thrust inherited structures which control the normal fault architecture, as well as the complex fault linkage and triggering of different fault segments. Moreover, the role of normal faults and the importance of strike-slip, thrusts and detachment structures, has not been clarified yet. More fieldwork is needed along with precise geophysical prospecting analysis, paleoseismological investigation of the faults, as well as re-evaluated seismological data in association with new ideas to better explain this new fault geometry complexity.

7. Acknowledgements

The authors would like to thank the Research Committee of the Aristotle University of Thessaloniki for the financial support of the field trips. We thank European Space Agency and PlanetLabs for providing satellite imagery. Two anonymous reviewers and the Editor-in-Chief of the Bulletin have greatly contributed to the improvement of the original manuscript and the authors greatly appreciate their input. Finally, the Embassy of Greece in Rome provided valuable assistance for acquiring a fieldwork permit during the second field trip.

8. References

Aki, K., 1966. Generation and propagation of G-waves from the Niigata earthquake of June 16, 1964. Estimation of earthquake movement, released energy and stress-strain drop from G-spectrum. *Bull. Earthq. Res. Inst.*, 44, 23-88.

Aringoli, D., Farabollini, P., Giacometti, M., Materazzi, M., Paggi, S., Pambianchi, G., Pierantoni, P.P., Pistolesi, E., Pitts, A., Tondi, E., 2016. The August 24th 2016 Accumoli earthquake: surface faulting and Deep-Seated Gravitational Slope Deformation (DSGSD) in the Monte Vettore area. *Annals of Geophysics*, 59, Fast Track 5.

Basili, R., Valensise, G., Vannoli, P., Burrato, P., Fracassi, U., Mariano, S., Tiberti, M.M., Boschi, E., 2008. The Database of Individual Seismogenic Sources (DISS), version 3: summarizing 20 years of research on Italy's earthquake geology. *Tectonophysics*, 453(1), 20-43.

Blumetti, A. M., Dramis, F., Michetti, A. M., 1993. Fault-generated mountain fronts in the central Apennines (Central Italy): Geomorphological features and seismotectonic implications. *Earth Surface Processes and Landforms*, 18(3), 203-223.

Boncio, P., Lavecchia, G., 2000. A structural model for active extension in Central Italy. *Journal of Geodynamics*, 29 (3), 233-244.

Boncio, P., Lavecchia, G., Milana, G., Rozzi, B., 2004. Seismogenesis in Central Apennines, Italy: an integrated analysis of minor earthquake sequences and structural data in the Amatrice- Campotosto area. *Annals of Geophysics*, 47(6), 1723-1742.

Borre, K., Cacon, S., Cello, G., Kontny, B., Kostak, B., Andersen, H.L., Moratti, G., Piccardi, L., Stemberk, J., Tondi, E., Vilimek, V., 2003. The COST project in Italy: analysis and monitoring of seismogenic faults in the Gargano and Norcia areas (central-southern Apennines, Italy). *Journal of Geodynamics*, 36 (1), 3-18.

Butler, R. W., Tavarnelli, E., Grasso, M., 2006. Structural inheritance in mountain belts: an Alpine–Apennine perspective. *Journal of Structural Geology*, 28(11), 1893-1908.

Calamita, F., Pizzi, A., 1992. Tettonica quaternaria nella dorsale appenninica umbro-marchigiana e bacini intrappenninici associati. *Studi Geologici Camerti*, Vol. Spec., 17-25.

Calamita, F., Pizzi, A., 1994. Recent and active extensional tectonics in the southern Umbro-Marchean Apennines (Central Italy). *Mem. Soc. Geol. It.*, 48, 541-548.

Calamita, F., Pizzi, A., Roscioni, M., 1992. I “fasci” di faglie recenti ed attive di M. Vettore-M. Bove e di M. Castello-M. Cardosa (Appennino umbro-marchigiano). *Studi Geologici Camerti*, 92(1), 81-95.

Calamita, F., Coltorti, M., Farabollini, P., Pizzi, A., 1994. Le faglie normali quaternarie nella dorsale appenninica umbro-marchigiana: proposta di un modello di tettonica di inversione. *Studi Geologici Camerti*, Vol. Spec. CROP, 18, 211-225.

Carafa, M., Bird, P., 2016. Improving deformation models by discounting transient signals in geodetic data: Geodetic data, stress directions, and long-term strain rates in Italy. *Journal of Geophysical Research: Solid Earth*, 121(7), 5557-5575.

Centamore E., Adamoli L., Berti D., Bigi G., Casnedi R., Cantalamessa G., Fumanti F., Morelli C., Micarelli A., Ridolfi M., Salvucci R., Chiocchini M., Mancinelli A., Potetti M., Chiocchini U., 1992. Carta geologica dei bacini della Laga e del Cellino e dei rilievi carbonatici circostanti (Marche meridionali, Lazio nord orientale, Abruzzo settentrionale). S.E.L.C.A., Firenze

Cheloni, D., Giuliani, R., D’Anastasio, E., Atzori, S., Walters, R.J., Bonci, L., D’Agostino, N., Mattone, M., Calcaterra, S., Gambino, P., Deninno, F., Maseroli, R., Stefanelli, G., 2014. Coseismic and post-seismic slip of the 2009 L’Aquila (central Italy) Mw 6.3 earthquake and implications for seismic potential along the Campotosto fault

from joint inversion of high-precision levelling, InSAR and GPS data. *Tectonophysics*, 622, 168-185. <http://dx.doi.org/10.1016/j.tecto.2014.03.009>

DISS Working Group, 2015. Database of Individual Seismogenic Sources (DISS), Version 3.2.0: A compilation of potential sources for earthquakes larger than M 5.5 in Italy and surrounding areas. <http://diss.rm.ingv.it/diss/>, Istituto Nazionale di Geofisica e Vulcanologia; DOI:10.6092/INGV.IT- DISS3.2.0.

EMERGEO, W.G.: Pucci, S., De Martini, P. M., Civico, R., Nappi, R., et al., 2016. Coseismic effects of the 2016 Amatrice seismic sequence: first geological results. *Annals of Geophysics*, 59, Fast Track 5.

Fortunato, C., Martino, S., Prestininzi, A., Romeo, R.W., Fantini, A., Sanandreas P., 2012. New release of the Italian catalogue of earthquake-induced ground failures (CEDIT). *Italian Journal of Engineering Geology and Environment*, DOI: 10.4408/IJEGE.2012-02.O-05.

Galadini, F., Galli, P., 2000. Active tectonics in the central Apennines (Italy)—input data for seismic hazard assessment. *Natural Hazards*, 22(3), 225-268.

Galadini, F., Galli, P., Moro, M., 2003. Paleoseismology of silent faults in the central Apennines (Italy): the Campo Imperatore fault (Gran Sasso Range fault system). *Annals of Geophysics*, 46(5), 11, 815-836.

Galli, P., Galadini, F., Calzoni, F., 2005. Surface faulting in Norcia (central Italy): a “paleoseismological perspective”. *Tectonophysics*, 403(1), 117-130.

Galli, P., Castenetto, S., Peronace, E., 2017. The Macroseismic Intensity Distribution of the 30 October 2016 Earthquake in Central Italy (Mw 6.6): Seismotectonic Implications. *Tectonics*, 36 (10), doi: 10.1002/2017TC004583

GSI—Geospatial Information Authority of Japan, 2016. Crustal Deformation Observed by Synthetic Aperture Radar (SAR). Online article and data at <http://www.gsi.go.jp/cais/topic160826-index-e.html>

Gruppo di lavoro IREA-CNR & INGV, 2016. Sequenza sismica di Amatrice: aggiornamento delle analisi interferometriche satellitari e modelli di sorgente, doi:10.5281/zenodo.61682

Hanks, T.C., Kanamori, H., 1979. A Moment Magnitude Scale. *J. Geophys. Res.*, 84(B5), 2348- 2350.

Hodgkinson, K. M., Stein, R. S., King, G. C., 1996. The 1954 Rainbow Mountain-Fairview Peak-Dixie Valley earthquakes: A triggered normal faulting sequence. *Journal of Geophysical Research: Solid Earth*, 101(B11), 25459-25471.

Huang, M. H., Fielding, E. J., Liang, C., Milillo, P., Bekaert, D., Dreger, D., Salzer, J., 2017. Coseismic deformation and triggered landslides of the 2016 Mw 6.2 Amatrice earthquake in Italy. *Geophysical Research Letters*, 44, doi:10.1002/2016GL071687.

IREA-CNR & INGV, 2017. Sequenza sismica del Centro Italia 2016-2017: aggiornamento delle analisi InSAR e modello preliminare di sorgente per gli eventi del 18/1/17. <http://doi.org/10.5281/zenodo.266966>

ITHACA, 2000. ITHACA Italy Hazard from Capable Faults: a database of active faults of the Italian onshore territory. A.M. Michetti, L. Serva and E. Vittori (eds.), CD-ROM and explication notes, ANPA; the updated version of the database is available online at http://www.isprambiente.gov.it/site/en-GB/Projects/ITaly_HAZards_from_CApable_faulting/default.html .

King, G. C., Stein, R. S., Lin, J., 1994. Static stress changes and the triggering of earthquakes. *Bulletin of the Seismological Society of America*, 84(3), 935-953.

Malinverno, A., Ryan, W. B., 1986. Extension in the Tyrrhenian Sea and shortening in the Apennines as result of arc migration driven by sinking of the lithosphere. *Tectonics*, 5(2), 227-245.

Marinkovic, P., Larsen, Y., 2016. Mapping and analysis of the Central Italy Earthquake (2016) with Sentinel-1 A/B interferometry [Dataset]. Zenodo. <http://doi.org/10.5281/zenodo.61133>.

Martino, S., F. et al., 2016. Landslides triggered by the August 24, 2016 (Mw 6.0) Amatrice earthquake (Italy): data survey and inventorying. Gruppo Nazionale di Geofisica della Terra Solida, 35th Convegno Nazionale, Lecce 22-24 November 2016.

Mariucci, M. T., Montone, P., 2016. Contemporary stress field in the area of the 2016 Amatrice seismic sequence (central Italy). *Annals of Geophysics*, 59, Fast Track 5.

Michele, M., Di Stefano, R., Chiaraluce, L., Cattaneo, M., De Gori, P., Monachesi, G., Latorre, D., Marzorati, S., Valoroso, L., Ladina, C., Chiarabba, C., 2016. The Amatrice 2016 seismic sequence: a preliminary look at the mainshock and aftershocks distribution. *Annals of Geophysics*, 59, Fast Track 5. <http://dx.doi.org/10.4401/ag-7227>

Okada, Y., 1992. Internal deformation due to shear and tensile faults in a half-space. *Bulletin of the Seismological Society of America*, 82(2), 1018-1040.

Pace, B., Peruzza, L., Lavecchia, G., Boncio, P., 2006. Layered seismogenic source model and probabilistic seismic-hazard analyses in central Italy. *Bulletin of the Seismological Society of America*, 96(1), 107-132.

Papadopoulos, G.A., Ganas, A., Agalos, A., Papageorgiou, A., Triantafyllou, I., Kontoes, Ch., Papoutsis, I., Diakogianni, G., 2017. Earthquake Triggering Inferred from Rupture Histories, DInSAR Ground Deformation and Stress-Transfer Modelling: The Case of Central Italy During August 2016–January 2017. *Pure Appl. Geophys.*, doi:10.1007/s00024-017-1609-8

Pauselli, C., Federico, C., Frigeri, A., Orosei, R., Barchi, M. R., Basile, G., 2010. Ground penetrating radar investigations to study active faults in the Norcia Basin (central Italy). *Journal of Applied Geophysics*, 72(1), 39-45.

Pavlidis, S., Papathanassiou, G., Georgiadis, G., Chatzipetros, A., Valkaniotis, S., 2016. Ground deformation observations of the August 24, 2016, Amatrice earthquake (central Italy). Report published online (<http://eqgeogr.weebly.com/blog/-amatrice>), Aristotle University of Thessaloniki, 10 pp. (in Greek).

Piccardi, L., A.M. Blumetti, V. Comerci, P. Di Manna, F. Fiumanti, L. Guerrieri, et al., 2016. The August 24, 2016, Amatrice earthquakes (Mw 6.0): field evidences of on-fault effects. (September 2016). <https://doi.org/10.5281/zenodo.155287>

Pierantoni, P., Deiana, G., Galdenzi, S., 2013. Stratigraphic and structural features of the Sibillini Mountains (Umbria-Marche Apennines, Italy). *Italian Journal of Geosciences*, 132(3), 497-520.

Pizzi, A., Galadini, F., 2009. Pre-existing cross-structures and active fault segmentation in the northern-central Apennines (Italy). *Tectonophysics*, 476(1), 304-319.

Pizzi, A., Calamita, F., Coltorti, M. A. U. R. O., Pieruccini, P., 2002. Quaternary normal faults, intramontane basins and seismicity in the Umbria-Marche-Abruzzi Apennine ridge (Italy): contribution of neotectonic analysis to seismic hazard assessment. *Boll. Soc. Geol. It., Spec. Publ*, 1, 923-929.

Pizzi, A., Di Domenica, A., Gallović, F., Luzi, L., Puglia, R., 2017. Fault Segmentation as Constraint to the Occurrence of the Main Shocks of the 2016 Central Italy Seismic Sequence. *Tectonics*, 36. <https://doi.org/10.1002/2017TC004652>.

Pucci, S., Mirabella, F., Pazzaglia, F., Barchi, M. R., Melelli, L., Tuccimei, P., Soligo, M., Saccucci, L., 2014. Interaction between regional and local tectonic forcing along a complex quaternary extensional basin: Upper Tiber Valley, Northern Apennines, Italy. *Quaternary Science Reviews*, 102, 111-132.

Reasenber, P. A., Simpson, R. W., 1992. Response of regional seismicity to the static stress change produced by the Loma Prieta earthquake. *Science*, 255 (5052), 1687-1690.

Roberts, G. P., Michetti, A. M., 2004. Spatial and temporal variations in growth rates along active normal fault systems: an example from The Lazio–Abruzzo Apennines, central Italy. *Journal of Structural Geology*, 26(2), 339-376.

Scisciani, V., 2009. Styles of positive inversion tectonics in the Central Apennines and in the Adriatic foreland: Implications for the evolution of the Apennine chain (Italy). *Journal of Structural Geology*, 31(11), 1276-1294.

Tavarnelli, E., 1996. The effects of pre-existing normal faults on thrust ramp development: an example from the Northern Apennines, Italy. *Geologische Rundschau*, 85(2), 363-371.

Toda, S., Stein, R. S., Richards-Dinger, K., Bozkurt, S. B., 2005. Forecasting the evolution of seismicity in southern California: Animations built on earthquake stress transfer. *Journal of Geophysical Research: Solid Earth*, 110 (B5), B05S16.

Toda, S., Stein, R. S., Sevilgen, V., Lin, J., 2011. Coulomb 3.3 graphic-rich deformation and stress-change software-user guide. U.S. Geological Survey Open-File Report 2011-1060, 63 pp.

Valensise, G., Vannoli, P., Basili, R., Bonini, L., Burrato, P., Carafa, M. M. C., Fracassi, U., Kastelic, V., Maesano, F.E., Tiberti, M.M. Tarabusi, G., 2016. Fossil landscapes and youthful seismogenic sources in the central Apennines: excerpts from the 24 August 2016, Amatrice earthquake and seismic hazard implications. *Annals of Geophysics*, 59, Fast Track 5.

Walker, J. F., Roberts, G. P., Cowie, P. A., Papanikolaou, I., Michetti, A. M., Sammonds, P., Wilkinson, M., McCaffrey, K.J.W., Phillips, R. J., 2012. Relationship between topography, rates of extension and mantle dynamics in the actively-extending Italian Apennines. *Earth and Planetary Science Letters*, 325, 76-84.

Wells, D. L., Coppersmith, K. J., 1994. New empirical relationships among magnitude, rupture length, rupture width, rupture area, and surface displacement. *Bulletin of the seismological Society of America*, 84 (4), 974-1002.

Zhang, Q. W., Zhang, P. Z., Wang, C., Wang, Y. P., Ellis, M. A., 2003. Earthquake triggering and delaying caused by fault interaction on Xianshuihe fault belt, southwestern China. *Acta Seismologica Sinica*, 16 (2), 156-165.